Demonstration of fast-electron populations in a low-pressure, low-power, magnetized RF plasma source

P. Jandovitz,[1,a)] C. Swanson,[1] J. Matteucci,[1] R. Oliver,[2] J. Pearcy,[3] and S. A. Cohen[1]
[1]*Princeton Plasma Physics Laboratory, Princeton University, Princeton, New Jersey 08543, USA*
[2]*Department of Physics, Brown University, Providence, Rhode Island 02912, USA*
[3]*Department of Physics, Princeton University, Princeton, New Jersey 08543, USA*

(Received 2 August 2017; accepted 10 March 2018; published online 27 March 2018)

Using x-ray spectroscopy, we demonstrate the existence of 0.3–6 keV electrons in a low-pressure, low-power, magnetized plasma source, heated by an external radio-frequency antenna located at one end of an axisymmetric tandem mirror. X-ray measurements on low-bulk-temperature, $T_{e,b} \sim 4$ eV, hydrogen, neon, argon, and gas-mixture plasmas show spectra with high-energy tails having a near-Maxwellian form with $T_{e,f}$ up to 650 eV. The fast electrons producing these x-rays have densities in the range of 10^7–10^9 cm^{-3}, 0.01%–1% of the bulk plasma density (up to 3×10^{11} cm^{-3}), and so carry a significant fraction of the plasma energy and represent an important mechanism relevant to power coupling and heat flow in similar plasma sources. *Published by AIP Publishing.* https://doi.org/10.1063/1.4998735

Low-temperature ($T_e < 10$ eV) plasmas are important due to their many applications in materials processing,[1] illumination,[2] and spacecraft propulsion,[3] as well as for answering questions of fundamental plasma physics. Radio-frequency (RF) plasma sources[4] are commonly used for studies of wave propagation, complex plasmas,[5] and wakefield acceleration. The properties of an RF plasma are largely determined by the mechanism of external power coupling. In this letter, we report on the existence of a significant population of keV electrons in a low-pressure, magnetized plasma source heated by an external antenna at one end of an axisymmetric tandem mirror. The fast electrons are indicative of an important and unexpected mechanism of power coupling that dramatically changes the plasma properties and the energy and particle fluxes in the system.

Energetic electrons in RF plasmas can cause many effects of practical importance. Fast electrons and the concurrent large floating potentials and x-ray emission may produce detrimental effects in semiconductor manufacturing, such as surface charging, arcing, and internal defects.[6] The fast electrons can also form ion-accelerating double-layer potential drops for propulsion applications.[7,8] Furthermore, fast electrons may prove valuable in diagnosing plasma properties, including magnetic topology[9] and non-adiabatic effects.

We begin with a brief discussion of RF discharge physics, with emphasis on suprathermal particles, followed by a description of our experimental setup. We then present x-ray spectra, count rates, time evolution, and spatial distributions for a variety of conditions. The paper ends with a qualitative explanation of the phenomenon and a brief discussion of open questions.

External antennae couple power to plasmas through their oscillating inductive and capacitive fields. Both forms of heating require some phase randomization mechanism for net power transfer: collisions with neutrals at high pressures or "collisions" with the sheath or skin-depth layer at low pressures.[10,11] Electrons heated by these mechanisms are limited to relatively low energies because the processes transfer energy incrementally and particles are lost or lose energy in elastic and inelastic collisions before they can gain large amounts of energy.

Fast electrons can be created in low-temperature discharges by secondary electron emission (SEE) from surfaces at large negative potentials. In high-pressure RF discharges, acceleration of secondary electrons (SEs) through high-voltage sheaths can be the dominant form of heating and ionization.[12] The transition between the ohmically heated α-mode and the SE-heated γ-mode corresponds to significant changes in the bulk plasma conditions.[13] However, in low-pressure discharges, SEs are usually considered insignificant because they are lost before they can interact with the plasma or gas.[14] The situation may be more complicated when electron reflection and magnetic effects are taken into account. A particle-in-cell simulation showed that plasma density significantly increased when electron reflection was considered, and high-energy electrons (up to 200 eV) existed throughout the plasma.[15]

Surfaces can be intentionally biased, as in DC or DC-RF discharges, or the potential can arise due to the difference in the mobility of ions and electrons, a phenomenon known as RF self-bias, whereby electrically floating surfaces near the antenna and exposed to the plasma develop a negative average potential approaching the amplitude of the driving voltage.[16] RF self-bias is exploited in reactive-ion etching and was shown to be the cause of wall heating near the antenna in a device similar to ours.[17] Boswell and Vender[18] reported the generation of an on-axis 1 μs-duration burst of electrons with 200 eV average energy at the initiation of helicon discharges and attributed it to ion-impact SEE, amplified by multipactoring between the antenna and a metal electrode 50–80 cm away.

Several groups[19] have reported the presence of static ion- and electron-accelerating double layers in helicon

a)pjandovi@pppl.gov

devices. One group observed an energetic ion beam, $\sim 10T_e$, and attributed it to a 0.1% population of 30 eV electrons in a 5 eV helicon-mode argon discharge in the Magnetic Nozzle Experiment (MNX).[20] The experiment described in this letter uses the same antenna, plasma formation region, and magnetic nozzle as MNX but with added x-ray diagnostics. Measurements on the Madison Helicon Experiment showed the presence of a 165-eV ion beam in a low-pressure, capacitively coupled helicon argon discharge.[21] The beam was attributed to a drop in plasma potential from the source to the expansion chamber, which they suggested was caused by RF self-bias.[22]

Our experimental setup is shown in Fig. 1. Gas is bled into the source end cell (SEC). At the left end of the SEC is a double-saddle antenna wrapped around a 3.8-cm-ID Pyrex pipe [see Fig. 1(c)]. The antenna is the inductor in a T-type tank circuit driven by a 10–1000 W, 27-MHz RF power supply. An electrically floating metal endplate, supporting a plasma-facing stainless steel and tungsten cup, closes one end of the Pyrex pipe. The other end connects to the grounded SEC vacuum vessel. The SEC is connected through a grounded 2-cm-ID aperture to the central cell (CC). The other end of the CC is connected to the far end cell (FEC), which contains a biasable Ta paddle. The plasma in the SEC was found to be insensitive to modest changes downstream, and so, the effects of the CC and FEC are not considered in this paper. The axial magnetic field is generated by four sets of coaxial electromagnet coils and the nozzle coils at the ends of the CC. Locations of B-field values are denoted by subscripts s, $z = -119$ cm, and n, $z = \pm 45$ cm, with $B_s \sim 100$–300 G ($f_{ce} \sim 300$–800 MHz) and $B_n \sim 1000$–3000 G. With the forward minus reflected power measured at the amplifier output, $P_{rf} \sim 200$ W, typical bulk plasma parameters are as follows: $T_e \approx 4$ eV; $n_e \approx 1 \times 10^{10}$ cm^{-3}; and floating potential ≈ -20 Volts, with the neutral density in the range of 0.3–30 $\times 10^{13}$ cm^{-3}. The plasma potential in the SEC was inferred from probe characteristics to be near ground. The bulk plasma in the SEC is described in more detail in an earlier publication.[8]

The primary diagnostics are an Amptek XR-100CR Si-PIN diode and a FAST silicon drift detector (SDD),[23] which are x-ray detectors. Due to window transmission, the PIN detectors have an ~900 eV low energy cutoff, while the SDD cutoff is ~300 eV. Detector lines-of-sight may be scanned across the plasma using movable slits. Partial pressures of gases were measured with a quadrupole residual gas analyzer in the FEC. Without cryopumping in the CC, H_2O and CO partial pressures were typically 10 and 5% of the working gas. With cryopumping, the total content of all impurity gases dropped to less than 1%. Because of the low degree-of-ionization, <1%, the majority of x-rays come from electrons scattered from the nuclei of neutral gas molecules rather than plasma ions. For the low-Z elements we consider, H, C, N, O, and Ne, the brightness of the Bremsstrahlung for $E > 1$ keV is proportional to Z^2 of the nucleus, independent of the state-of-ionization.

Figure 2(a) shows x-ray spectra obtained by the Si-PIN detector from hydrogen and argon plasmas in the SEC, corrected for the transmission efficiency of its Be window. In both cases, significant x-ray emission occurs in the 1.0–5.0 keV range, characterized by a ~400 eV exponential tail above 2 keV. For the argon plasma, a prominent peak comprising two unresolved lines, Ar K_α (2.96 keV) and K_β (3.19 keV), appears near 3 keV. The presence of this peak is convincing evidence that the fast electrons interact with the neutral fill gas, supporting our interpretation of the observed x-rays as arising from gas-target bremsstrahlung in the plasma column as opposed to solid-target bremsstrahlung at the system walls. Using the Elwert approximation for the bremsstrahlung cross-section,[24] the fast electron density was estimated to be $\sim 4 \times 10^7$ cm^{-3} for energies greater than 1.9 keV, showing that ~30% of this plasma's energy is in the fast electrons. The collision time for such electrons is >0.1 s, much longer than the observed time for the discharge to reach the steady-state and to decay when the RF power is stopped. The exponential characteristic of the x-ray spectrum, as opposed to the sharp cutoff expected from electrons accelerated by a DC or sinusoidal potential, points to the importance of collisionless relaxation or stochastic heating mechanisms in generating a Maxwellian-like electron distribution in this system. Figure 2(b) shows an SDD-obtained spectrum with the Ne plasma. The better low-energy

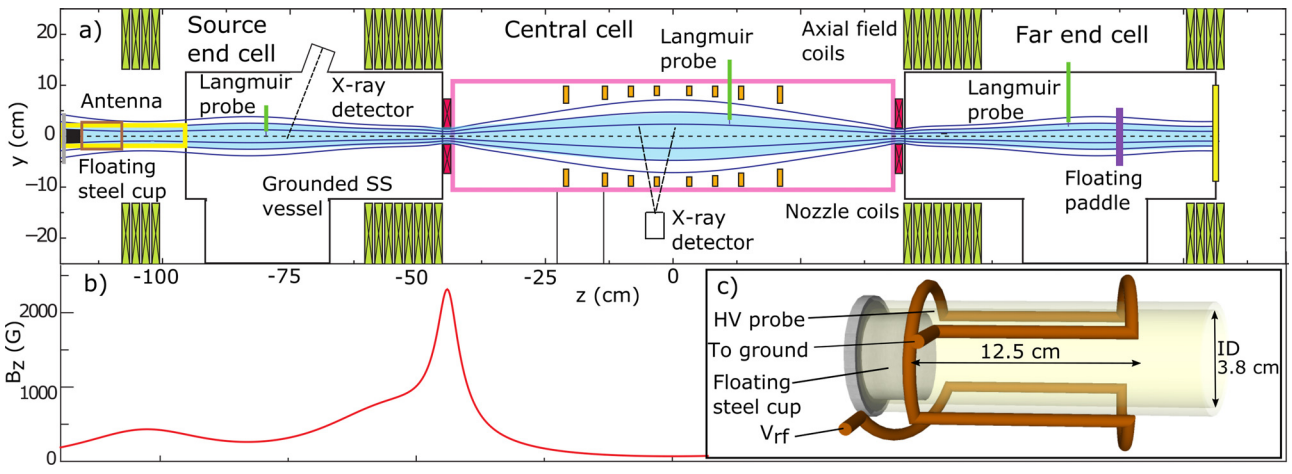

FIG. 1. (a) Schematic of the experiment. (b) Typical on-axis axial field magnitude *versus* z. (c) Source region with a double-saddle antenna.

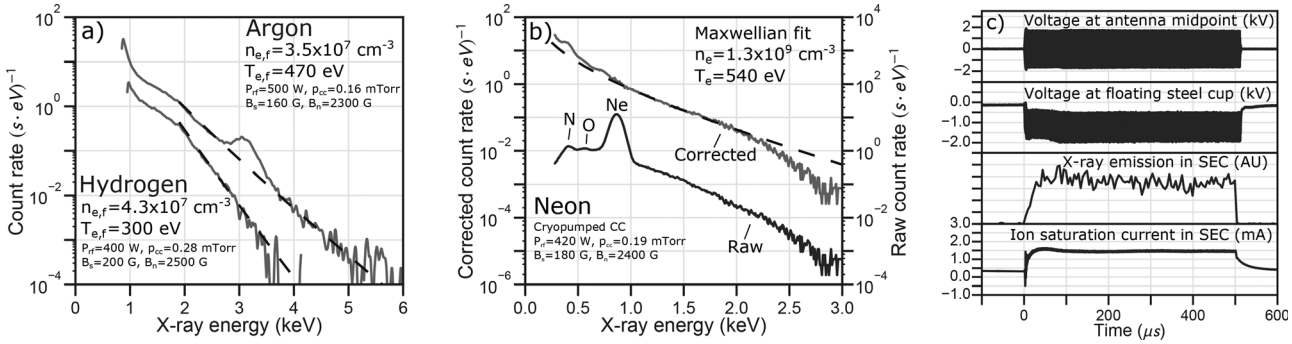

FIG. 2. (a) X-ray spectra from H_2 and Ar plasmas in the SEC, using an Si-PIN detector. (b) X-ray spectrum from the Ne plasma in the SEC, using an SDD detector. The corrected spectrum was obtained by subtracting a Gaussian approximation of the neon peak and correcting for the window transmission. The quoted electron densities refer to electrons with energies above 1.9 keV in (a) and above 250 eV in (b). The fits were obtained using the Elwert approximation for the Bremsstrahlung cross-section. (c) Time evolution parameters when RF power is modulated at 1 kHz. H_2 plasma, $P_{rf} = 400$ W, $B_s = 170$ G, $B_n = 2300$ G, and $p_{cc} = 0.90$ mTorr.

transmission of its window allows probing deeper into the bulk electron energy distribution, showing that the Maxwellian characteristic does extend to lower energies, which leads to a density estimate of $\sim 10^9\,\mathrm{cm}^{-3}$ or $\sim 1\%$ of the bulk density. At these temperatures and densities, the ionization rate due to the fast electrons is comparable to that due to the bulk electrons, showing the potential importance of the fast electrons in determining the plasma properties. Despite this, a discontinuous transition to a lower bulk-temperature state, as in the traditional γ-mode, was not observed.

When the RF power to the antenna is a square-wave modulated at 1 kHz, parameters of the discharge change with time. Figure 2(c) shows the time evolution of four parameters. The antenna voltage, measured at its midpoint, oscillates at 27 MHz, achieving a 4 kV peak-to-peak value in a few μs. The highest voltage point on the antenna is 1.9 times higher. According to a simple model of asymmetric self-bias from a sinusoidal driving voltage, the wall near this point would self-bias to as high as $-V_{pp}/2 = -3.8$ kV DC.[25] Secondary electrons emitted from the wall could gain energies up to $V_{DC} + V_{pp}/2 = 5.7$ keV depending on the phase of the RF voltage.

Under the same conditions, the steel cup (SC) that closes the left end of the source tube was found to float to a mean potential of -1.2 kV, reaching that value in ~ 10 μs. The steel cup is then also a potential source of energetic secondary electrons. In contrast to the RF antenna potential, the cup's floating voltage shows RF oscillations that never reach ground. Thus, unless the plasma potential near the cup is very negative, the cup must be a net sink of fast electrons to maintain its negative charge. After the cessation of RF power, the steel-cup voltage falls to near ground within 10 μs.

X-ray emission in the SEC begins very soon after the RF power is turned on, levels off within 15 μs, and decays within 10 μs of the cessation of RF power. The x-ray spectrum remains roughly constant over the discharge, indicating that the high-energy tail reaches a steady-state much more quickly than the collisional equilibration time. The plasma density in the SEC, inferred from the ion saturation current, was approximately constant at $4 \times 10^{11}\,\mathrm{cm}^{-3}$ during the RF pulse.

Fast electrons generated by emission from the Pyrex pipe near the antenna should be concentrated at the edge of the plasma column due to the magnetic field (the gyro-radius of 1-keV electrons is 5 mm in the magnetic field near the antenna). However, as Fig. 3(a) shows, x-ray emission is concentrated in the center of the plasma column. In addition, fast electrons originating from the Pyrex would have their energy primarily perpendicular to the magnetic field. Figure 3(b) shows that x-ray emission in the SEC is unaffected by changes in the nozzle field, suggesting that confinement of fast electrons at the nozzle is unaffected in this range. This is consistent with the fast electrons having mostly perpendicular energy, and so, they are almost always reflected at the nozzle and are lost to other surfaces. However, it is also consistent with the fast electrons having mostly parallel energy, such as those emitted from the steel cup, which would almost always pass through the nozzle. The density of fast electrons

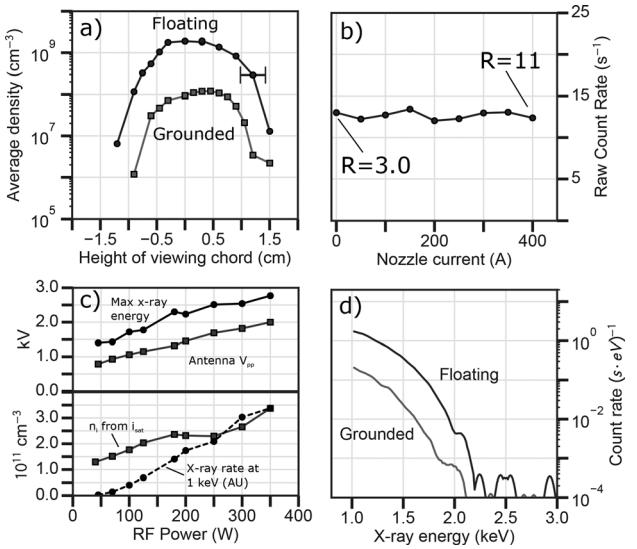

FIG. 3. (a) Transverse spatial scan with a floating and grounded steel cup. H_2 plasma, $P_{rf} = 300$ W, $B_s = 220$ G, $B_n = 2500$ G, and $p_{cc} = 0.36$ mTorr. (b) X-ray count rate in the SEC vs. nozzle current. H_2 plasma, $P_{rf} = 190$ W, $B_s = 290$ G, and $p_{cc} = 0.86$ mTorr. H_2 plasma, $P_{rf} = 300$ W, $B_s = 220$ G, $Bn = 2500$ G, and $p_{cc} = 0.60$ mTorr. (c) RF power scan showing maximum observed x-ray energy, peak-to-peak voltage measured at the midpoint of the antenna, the x-ray count rate at 1 keV, and the bulk ion density. H_2 plasma, $B_s = 170$ G, $B_n = 2300$ G, and $p_{cc} = 0.9$. (d) X-ray spectra in the SEC with a floating and grounded steel cup. H_2 plasma, $P_{rf} = 205$ W, $B_s = 180$ G, $B_n = 2300$ G, and $p_{cc} = 0.7$ mTorr.

in the CC is ~10% that in the SEC, consistent with flow through the nozzle and along the expanding field lines. However, x-ray measurements in the CC indicate significant trapping and confinement of fast electrons in the CC mirror, and so, the relatively low density of fast electrons in the CC is consistent with particle loss to surfaces in the source and SEC dominating loss through the nozzle.[26]

Grounding the steel cup causes the x-ray emission in the SEC to drop by a factor of ~10, as seen in Figs. 3(a) and 3(d). However, the shape of the spectrum does not change significantly, suggesting that the floating steel cup is not essential to the fast electron generation process. Additionally, the transverse emission profile, Fig. 3(a), remains peaked on axis when the cup is grounded. Figure 3(c) shows that the maximum observed x-ray energy correlates well with the peak-to-peak voltage at the midpoint of the antenna, but the x-ray energy is consistently ~1.5 times higher. According to the simple model of self-bias, surfaces near the antenna will reach a peak negative voltage of $-V_{pp}$. Since the voltage at the midpoint is roughly half of the maximum antenna voltage, it is plausible that there are Pyrex surfaces that reach potentials above the maximum observed x-ray energy. Both the x-ray count rate and bulk density smoothly increase as the RF power increases, but the x-ray count rate increases slightly faster, consistent with a rise in $T_{e,f}$.

Figure 4(a) shows that the average voltage of the steel cup (SC) is also strongly correlated with the maximum observed x-ray energy. However, the maximum voltage the cup reaches is lower than the maximum x-ray energy, and so, the high-energy tail cannot be explained by simple emission from the cup.

Figures 4(b)–4(d) show the effects on x-ray emission of changing the CC neutral pressure. Since the observed x-rays are predominantly produced by electron-neutral collisions, a decrease in pressure should contribute to a linear decrease in x-ray emission. However, Fig. 4(b) shows that, for hydrogen plasmas, decreasing the neutral pressure causes a steady and significant increase in emission until the discharge is not sustainable, typically below 0.2 mTorr. Figure 4(d) shows spectra for three hydrogen pressures. The increase in emission at lower pressure can be explained by the increase in $T_{e,f}$, which leads to an exponential increase in the fraction of x-ray producing electrons. The case for Ar plasmas, shown in Fig. 4(c), is more complicated. There is no smooth extended trend *vs* pressure as in the case of hydrogen. For argon, x-rays are only observed in a more limited pressure range. Below 0.1 mTorr, Ar discharges are not sustained, and above 0.6 mTorr, the discharge transitions to a "blue-core" helicon mode, wherein the antenna and the steel-cup voltages are significantly lower and no x-rays are observed.

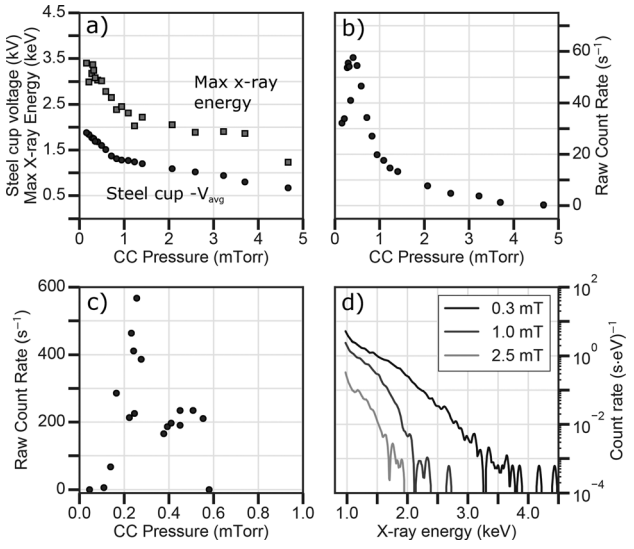

FIG. 4. (a) Steel cup floating voltage (SC) and maximum x-ray energy *vs* hydrogen pressure. X-ray count rate vs. neutral pressure for (b) H_2 plasmas and (c) Ar plasmas is shown. (d) X-ray spectra at three hydrogen pressures. (a), (b), and (d): H_2 plasma, $P_{rf} = 390$ W, $B_s = 220$ G, and $B_n = 2500$ G; and (c): Ar plasma, $P_{rf} = 300$ W, $B_s = 200$ G, and $B_n = 2400$ G.

Although the nearly wall-parallel magnetic field promotes the return to the Pyrex pipe of electrons emitted from there, other processes can work against this. The voltage at different points on the Pyrex inner surface varies considerably because of the inductive voltage drop along the antenna and its winding pattern. SEs that are emitted at a less negative voltage than they see upon return will be reflected by the sheath, while those emitted at a more negative voltage will return to the surface, likely causing significant electron-impact SEE. Electrons that reflect from the sheath can be coherently energized, as in the Lieberman model, as well as directed inward to a smaller radius. Additionally, there is a weak, R = 1.2, magnetic mirror shortly downstream from the antenna, which could reflect the fast electrons depending on how much parallel energy they gain, and a stronger, R = 10, mirror at the nozzle that would reflect almost all of the fast electrons. Consideration of these effects, anomalous transport, and self-consistent sheath formation may significantly change the model predictions, and so, further investigation is necessary.

In summary, x-ray emission provides indisputable evidence for keV electron populations in low-power, low-temperature, magnetized discharges. The clear evidence of fast electrons observed in this system raises the possibility of similar large, unaccounted for effects in systems in research and industry. At their observed levels of 0.01%–1% of the bulk density, too low to be seen *via* common probe diagnostics,[27] the fast electrons carry a significant portion of the plasma energy and will significantly affect the power balance of the system, heat flow, wave propagation, ionization, and excitation.

We thank Dr. E. Startsev and Dr. I. Kaganovich for useful conversations and Mr. B. Berlinger for technical support. This work was supported, in part, by DOE Contract No. DE-AC02-09CH11466.

[1]M. A. Lieberman and A. J. Lichtenberg, *Principles of Plasma Discharges and Materials Processing* (John Wiley & Sons, 2005).
[2]P. Flesch, *Light and Light Sources: High-Intensity Discharge Lamps* (Springer-Verlag, Berlin, 2007).
[3]E. Choueiri, *Physics of Plasma Propulsion* (CRC Press, 2014).
[4]Y. P. Raizer, M. N. Shneider, and N. A. Yatsenko, *Radio-Frequency Capacitive Discharges* (CRC Press, 1995).
[5]G. Morfill and A. Ivlev, Rev. Mod. Phys. **81**, 1353 (2009).
[6]J. Zhang, E. Fretwurst, R. Klanner, H. Perrey, I. Pintilie, T. Poehlsen, and J. Schwandt, J. Instrum. **6**, C11013 (2011).

[7]N. Singh, Phys. Plasmas **18**, 122105 (2011).
[8]X. Sun, S. A. Cohen, E. E. Scime, and M. Miah, Phys. Plasmas **12**, 103509 (2005).
[9]J. Matteucci and S. Cohen, Bull. Am. Phys. Soc. **60**, 41 (2015).
[10]V. A. Godyak, Sov. Phys. - Tech. Phys. **16**, 1073 (1972).
[11]M. A. Lieberman and V. A. Godyak, IEEE Trans. Plasma Sci. **26**, 955 (1998).
[12]S. M. Levitskii, Sov. Phys.-Tech. Phys. **2**, 887 (1957).
[13]V. A. Godyak and A. S. Khanneh, IEEE Trans. Plasma Sci. **14**, 112 (1986).
[14]G. R. Misium, J. Vacuum Sci. Technol. A: Vac., Surf., Films **7**, 1007 (1989).
[15]R. Krimke and H. M. Urbassek, J. Phys. D: Appl. Phys. **29**, 378 (1996).
[16]V. A. Godyak and N. Sternberg, Phys. Rev. A **42**, 2299 (1990).
[17]C. Charles, R. W. Boswell, and M. A. Lieberman, Phys. Plasmas **10**, 891 (2003).
[18]R. Boswell and D. Vender, Plasma Sources Sci. Technol. **4**, 534 (1995).
[19]C. Charles, Plasma Sources Sci. Technol. **16**, R1 (2007).
[20]S. A. Cohen, X. Sun, N. M. Ferraro, E. E. Scime, M. Miah, S. Stange, N. S. Siefert, and R. F. Boivin, IEEE Trans. Plasma Sci. **34**, 792 (2006).
[21]M. Wiebold, Y.-T. Sung, and J. E. Scharer, Phys. Plasmas **18**, 063501 (2011).
[22]M. Wiebold, Y.-T. Sung, and J. E. Scharer, Phys. Plasmas **19**, 053503 (2012).
[23]J. Pantazis, *Amptek: X-Ray Detectors* (Amptek, Bedford, MA, 2016).
[24]G. Elwert, Ann. Phys. **34**, 178 (1939).
[25]P. Chabert and N. Braithwaite, *Physics of Radio-Frequency Plasmas* (Cambridge University Press, 2011).
[26]C. Swanson, P. Jandovitz, and S. A. Cohen, AIP Adv. **8**, 025222 (2018).
[27]V. A. Godyak and B. M. Alexandrovich, J. Appl. Phys. **118**, 233302 (2015).